Applied Catalysis B: Environmental 138–139 (2013) 333–341

Contents lists available at SciVerse ScienceDirect

Applied Catalysis B: Environmental

journal homepage: www.elsevier.com/locate/apcatb

Heterogeneous photocatalysis of moxifloxacin: Identification of degradation products and determination of residual antibacterial activity

Xander Van Doorslaer[a], Kristof Demeestere[a], Philippe M. Heynderickx[a], Marieke Caussyn[a], Herman Van Langenhove[a], Frank Devlieghere[b], An Vermeulen[b], Jo Dewulf[a,*]

[a] Research Group EnVOC, Department of Sustainable Organic Chemistry and Technology, Faculty of Bioscience Engineering, Ghent University, Coupure Links 653, B-9000 Ghent, Belgium
[b] Laboratory of Food Microbiology and Food Preservation, Department of Food Safety and Food Quality, Faculty of Bioscience Engineering, Ghent University, Coupure Links 653, B-9000 Ghent, Belgium

ARTICLE INFO

Article history:
Received 19 January 2013
Received in revised form 1 March 2013
Accepted 5 March 2013
Available online 14 March 2013

Keywords:
Heterogeneous photocatalysis
Fluoroquinolone
Pathway
Degradation products
Antibacterial activity

ABSTRACT

TiO_2-mediated heterogeneous photocatalysis of the fluoroquinolone antibiotic moxifloxacin in water is investigated with respect to both the formation of degradation products and the evaluation of residual antibacterial activity after photocatalytic treatment. High-resolution magnetic sector mass spectrometry coupled to high performance liquid chromatograph is used to determine the accurate mass of the measured degradation products. Eight main photoproducts are identified at both acidic, neutral and alkaline pH. A molecular structure is proposed by using the accurate mass, the double bond equivalent and by taking into account the structural formula of the parent compound. The photocatalytic degradation does not take place at the quinolone core and defluorination was not observed. A general initial photocatalytic pathway for moxifloxacin is proposed. Time profiles of the different degradation products reveal that the solution pH influences their relative abundance during reaction but the observed degradation products show no pH dependency. Residual antibacterial activity of the photocatalytic reaction solutions against *Escherichia coli* (G^-), *Staphylococcus carnosus* (G^+), *Streptococcus mutans* (G^+) and *Klebsiella pneumoniae* (G^-) is evaluated by means of agar diffusion tests. A reduction in antibacterial activity is noticed for all investigated pH levels with a complete inactivation at neutral pH after 12 min of photocatalytic treatment.

1. Introduction

Fluoroquinolones (FQs) are a class of synthetic broad-spectrum antibacterial agents used for human, veterinary and aquaculture applications. As a result of their rising popularity, an increasing amount of FQ antibiotic residues is detected in effluent waters of common wastewater treatment plants (WWTPs) [1–3]. A continuous input of low concentrations in WWTPs provides suitable conditions for the selective pressure toward resistant organisms [4,5]. Next to resistance formation, the possible toxic effects provoked on fauna and flora are of increased concern [6,7].

Therefore, physical-chemical removal technologies are needed such as advanced oxidation processes (AOP) like heterogeneous photocatalysis, ozonation and sonication [8–13]. AOPs oxidize the compounds through active species like hydroxyl radicals generated at ambient conditions. The photocatalytic degradation of FQs is not widely studied, especially for the more recently introduced FQs like moxifloxacin (MOX), see Fig. 1, which accounts for 81.3% of the European third generation quinolone outpatient consumption in 2009 [14]. To evaluate the efficiency of an AOP, not only kinetics and process parameters are of interest, it is equally important to study the formed degradation products and residual antibacterial activity after an AOP treatment [15–20].

The scope of this manuscript is to gain new mechanistic insights in the photocatalytic degradation of MOX as a relevant model compound and primarily focusses on the composition of the water phase during this reaction. In a first part it deals with (i) the identification of the main photocatalytic degradation products of MOX, (ii) elucidation of the possible photocatalytic degradation pathway, and (iii) evaluating the effect of pH on this matter. Secondly, the residual antibacterial activity of the reaction solution is

* Corresponding author at: Coupure Links 653, B-9000 Ghent, Belgium. Tel.: +32 9 264 59 49; fax: +32 9 264 62 43.
E-mail address: Jo.Dewulf@UGent.be (J. Dewulf).

0926-3373/$ – see front matter © 2013 Elsevier B.V. All rights reserved.
http://dx.doi.org/10.1016/j.apcatb.2013.03.011

Nomenclature

Roman symbols

C	concentration, M
n_{rep}	number of repetitions, –
t_R	retention time, min

Greek symbols

θ	theta angle,°

Subscripts

cat	catalyst
liq	liquid phase
0	initial

Acronyms and abbreviations

AOP	advanced oxidation processes
BHI	brain hearth infusion
Da	Dalton
DBE	double bond equivalent
DNA	desoxyribonucleic acid
ESI	electrospray ionization
FQ	fluoroquinolone
FWHM	full width at half maximum
HPLC	high performance liquid chromatography
HR-MS	high resolution mass spectrometry
LR-MS	low resolution mass spectrometry
MOX	moxifloxacin
MS	mass spectrometry
NA	nutrient agar
PDA	photo diode array
PEG	polyethylene glycol
rps	rotations per second
S/N	signal to noise ratio
TSA	tryptone soy agar
UV	ultra violet
WWTP	wastewater treatment plant

examined during the photocatalytic process at different reaction pH for a representative set of bacteria.

Newly identified photocatalytic degradation products and a more elaborate degradation pathway are proposed here, and – to the author's best knowledge – this is the first time that the effect of pH on the degradation products and their residual antibacterial activity is studied for this third generation fluoroquinolone.

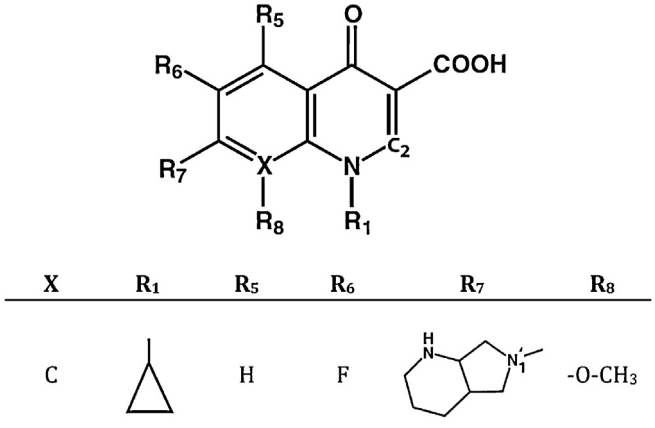

Fig. 1. General molecular structure of the quinolone moiety with substituents for the fluoroquinolone moxifloxacin.

2. Procedures

2.1. Chemicals

Moxifloxacin.HCl, BAY12-80369, is provided by Bayer (Germany). KH_2PO_4 (Sigma-Aldrich, 99%), K_3PO_4 (Sigma–Aldrich, ≥98%), NaOH (Acros), K_2HPO_4 (Acros, ≥98%) and concentrated H_3PO_4 (Merck, 85%) are used for pH adjustment. All stock and buffer solutions are prepared with deionized water and all reagents are used as received without any purification. As a photocatalyst, commercial Degussa P25 TiO_2 is used with a BET specific surface area of $48.3 \pm 0.7\ m^2\ g^{-1}$ (TRISTAR Micromeritics), $86.7 \pm 0.6\%$ of anatase with primary anatase and rutile particle sizes of 18.7 ± 0.1 nm and 23.3 ± 1.2 nm, respectively (Siemens D5000 scintillation counter, $\theta = 0.02°$) [21]. Pure air ($20 \pm 1\%\ O_2$) is purchased from Air Liquide (Belgium).

Nutrient agar (NA), Tryptone soy agar (TSA) and brain heart infusion (BHI) is purchased from OXOID LTD (UK). NaCl (99.5%) used in the physiological solution is provided by Sigma–Aldrich.

2.2. Degradation experiments

Photocatalytic degradation experiments are performed at ambient reaction conditions in a lab scale batch slurry reactor with a diameter and height of 7 and 10 cm, respectively. A UV-A pen ray (300–440 nm with main peak at 365 nm), provided by UVP (United Kingdom), is used as the light source during photocatalytic degradation experiments and is positioned axially in the reactor. The applied operational variables in this study are mentioned in Table 1. The selected conditions are a result of recent optimization work on the photocatalytic degradation of moxifloxacin, as described in detail in Van Doorslaer et al. [11,22]. The solution is continuously stirred and sparged with air. Adsorption/desorption equilibrium is attained during 30 min in the dark before switching on the lamp to start the degradation reaction. A sample of the solution is taken at 0 min reaction time, representing the solution before catalyst addition, and 0′ min reaction time, representing the starting point for the reaction after adsorption/desorption equilibrium. During degradation, samples are taken at regular time intervals, filtered and analyzed by HPLC–PDA/MS, see Section 2.3.

2.3. Identification of degradation products

An initial concentration of 124.6 μM MOX (Table 1) is used during the photocatalytic degradation experiments performed to identify its degradation products. This rather high concentration is chosen for the reason that it simplifies the detection of the degradation products without any preconcentration steps in which some

Table 1
Experimental conditions applied during heterogeneous photocatalytic degradation of MOX.

Process variable	Unit	Value
Initial concentration, $C_{0,MOX}$	μM	37.4[a] and 124.6[b]
Temperature	K	298
pH	–	3.0, 7.0 and 10.0
Stirring speed	rps	13.2
Reactor volume	mL	200
Catalyst loading, C_{cat}	$g\ L^{-1}$	1.0
Air flow	$mL\ min^{-1}$	60
Phosphate buffer concentration	mM	10
Light intensity UV-A	mW	104

[a] Concentration applied during photocatalytic degradation for the antibacterial diffusion tests.
[b] Concentration applied during photocatalytic degradation for the determination of degradation products.

of the products may be overlooked because of selectivity during sample pretreatment. Aqueous samples of 1 mL are taken at 0, 0′, 5, 15, 25, 35, 45, 55, 65, 75, 85, 95, 105, 115, 125, 135 and 145 min of photocatalytic degradation time, filtered over a 0.2 μm disk filter with a regenerated cellulose membrane (Spartan) and analyzed by HPLC-ESI-MS. The HPLC is equipped with a Luna C18(2) column (150 mm × 2.0 mm, 3 μm, Phenomenex, USA), maintained at 35 °C, and a binary mobile phase consisting of 0.1% formic acid in water and 0.1% formic acid in methanol is used. The mobile phase flow rate was 170 μL min^{-1} and starts with one minute isocratic 10% organic phase, which then rises to 60% in 20 min and to 100% in the following five minutes. It was kept constant for 10 min before returning to the starting condition in 1 min. It was then equilibrated for 20 min prior to the next run. The MS detection is performed on a Thermo Finnigan double focusing magnetic sector MAT95XP-TRAP high resolution mass spectrometer (Finnigan, Bremen, Germany) equipped with an electrospray ionization (ESI) source in positive-ion mode. The spray voltage was 3 kV with nitrogen as sheath gas at 4 bars and a capillary temperature of 250 °C.

Low resolution magnetic scan is used during the initial analysis of the photocatalytic samples taken at preset reaction times. To elucidate the molecular composition of the measured degradation products, high resolution measurements are performed, with a mass resolution of 10,000 (10% valley definition, corresponding to 20,000 mass resolution at full width at half maximum (FWHM)), on the sample taken at the reaction time where most degradation products with an ion intensity greater than 10^5 μV were observed during low resolution modus. Polyethylene glycols (PEG) were used as high resolution mass spectrometry (HR-MS) internal mass calibration standards for determination of the accurate mass and chemical formula of the degradation products. Given the molecular formula of protonated moxifloxacin ($C_{21}H_{25}O_4N_3F$), chemical formulae containing 0–21 carbon atoms, 0–30 hydrogen atoms, 0–10 oxygen atoms, 0–3 nitrogen atoms, and 0–1 fluoro atoms were taken into account for identification of degradation products.

2.4. Antibacterial activity

Non-pathogenic bacteria *Escherichia coli* LMG 8223 (G^-), *Staphylococcus carnosus* LFMFP 163 (G^+), *Streptococcus mutans* LMG 14558T (G^+) and *Klebsiella pneumoniae* LMG 2095 (G^-) were used. The sensitivity of the selected bacteria to MOX is tested through agar diffusion tests using a concentration range of 12.46, 7.48, 2.49, 1.25, 0.75 and 0.07 μM of the pure substance moxifloxacin. Agar diffusion tests are performed using pour plates consisting of 2.8% nutrient agar and for all investigated bacteria the same initial cell density is applied (10^8 cells mL^{-1} broth). The nutrient agar is buffered by peptones present in the nutrient agar mix. Wells of 0.64 cm diameter were cut manually in the agar. To evaluate the residual antibacterial activity during the photocatalytic degradation of MOX at pH 3.0, 7.0 and 10.0, samples of 2 mL are taken at 0, 0′, 2, 4, 6, 8, 10, 12 and 14 min degradation time, filtered over a 0.2 μm disk filter and 1/3 diluted before dosing 20 μL in the wells. Degradation experiments were performed in triplicate and separately evaluated. Inhibition zones of both experiments are measured after 48 h incubation at 37 °C in aerobic conditions with a digital slide gauge. The inhibition zone at 0′ min degradation time represents 100% residual inhibition. Inhibition zones measured after *X* minutes of photocatalytic degradation time are divided by the inhibition zone diameter at 0′ min degradation time and expressed as residual percentage of antibacterial activity. An exemplary calculation is made in supporting information.

3. Results and discussion

3.1. Identification of degradation products

In this section the effect of reaction solution pH on the degradation product formation is studied. The importance of the FQ and catalyst dissociation state on the photocatalytic degradation of MOX is investigated in recently published work [11]. A preliminary photolytic experiment under the same reaction conditions as mentioned in Section 2.2 showed that the amount of photolytic MOX degradation was below 5%. Photocatalytic degradation of a 124.6 μM MOX solution in deionized water at pH 3.0, 7.0 and 10.0 results in a large number of degradation products. The time course of the HPLC-MS peak areas associated with these products during MOX degradation together with the residual MOX concentration in solution at pH 7.0, are presented in Fig. 2. Similar figures for pH 3.0 and 10.0 are added in supporting information (Figs. SI-1 and SI-2). At pH 7.0, fourteen different degradation products with a signal-to-noise ratio (S/N) higher than ten are clearly detected during low resolution analysis with several of them having the

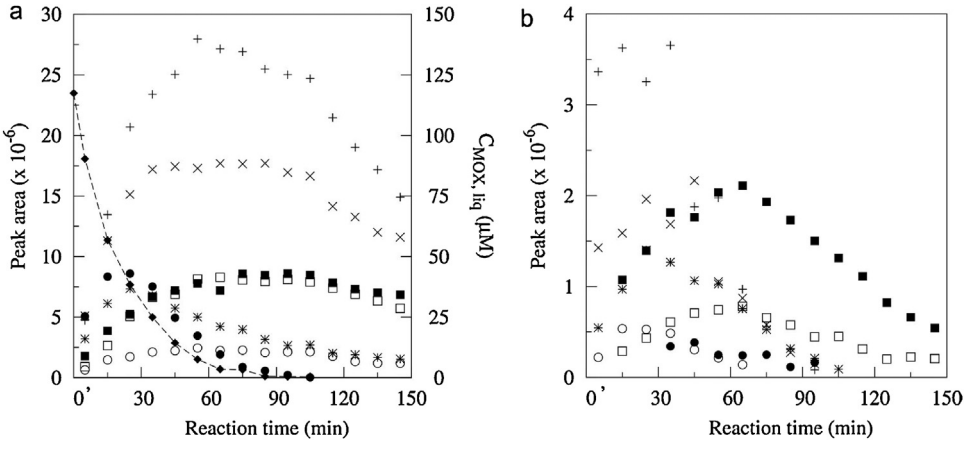

Fig. 2. A: Integrated peak areas of the major products in the liquid phase during the photocatalytic degradation of MOX with $C_{0,MOX}$ = 124.6 μM, C_{cat} = 1.0 g L^{-1} P25, pH 7.0, T = 298 K, 13.2 rps, 60 ml min^{-1} air. Nominal masses (Da) and chromatographic retention time (t_R: min) are (+) 292, t_R: 23.46; (○): 306, t_R: 23.43; (■): 306, t_R: 22.11; (×): 320, t_R: 20.87; (●): 417, t_R: 16.00; (□): 429, t_R: 17.16 and (✱): 429, t_R: 12.11 (left *y*-axis), with (♦): the liquid concentration of MOX ($C_{MOX,liq}$ mg L^{-1}) during photocatalytic degradation (6% adsorption; n_{rep} = 1; right *y*-axis). Dashed line is plotted to guide the eye. b: Integrated peak areas of the minor products the liquid phase during the photocatalytic degradation of MOX with nominal masses (Da) and chromatographic retention time (t_R: min) are (+): 399, t_R: 15.89; (×): 399, t_R: 17.19; (✱): 399, t_R: 20.52; (□) 415, t_R: 10.74; (■): 415, t_R: 14.38; (○): 415, t_R: 17.40 and (●): 415, t_R: 21.46 (n_{rep} = 1).

Table 2
Determination of degradation products[a] of MOX after photocatalytic degradation at pH 3.0, 7.0 and 10.0 ($C_{0,MOX}$ = 124.6 μM, T = 298 K, 13.2 rps, 60 ml min^{-1} air, C_{cat} = 1.0 g L^{-1}) determined by HPLC and LR and HR mass spectrometry (n_{rep} = 1).

LR-MS				HR-MS							
Nominal mass (Da)	t_R[b] (min) pH 3	t_R[b] (min) pH 7	t_R[b] (min) pH 10	$[M+H]^+$ measured pH 3 (error[c] (ppm))	$[M+H]^+$ measured pH 7 (error[c] (ppm))	$[M+H]^+$ measured pH 10 (error[c] (ppm))	DBE[d]	Molecular formula	Difference with MOX		No.[a]
292	23.27	23.46	23.40	293.09304 (−0.59)	293.09047 (2.93)	293.09296 (−0.86)	9.0	$C_{14}H_{14}O_4N_2F$	−7C 11H N		12
306	22.46	22.11	22.02	no HR-MS	307.07148 (−3.25)	no HR-MS	10.0	$C_{14}H_{12}O_5N_2F$	−7C 13H N	+O	10
	23.30	23.43	23.33	no HR-MS	307.10788 (−3.20)	no HR-MS	9.0	$C_{15}H_{16}O_4N_2F$	−6C 9H N		8
320	20.68	20.87	20.75	321.08792 (−0.65)	321.08824 (0.35)	321.08815 (0.07)	10.0	$C_{15}H_{14}O_5N_2F$	−6C 11H N	+O	11
399	15.73	15.89	15.85*	400.16774 (2.57)	400.16801 (3.25)	no HR-MS	12.0	$C_{21}H_{23}O_4N_3F$	−2H		6
	16.78	n.d.	16.44	no HR-MS	no HR-MS	400.16882 (5.27)	12.0	$C_{21}H_{23}O_4N_3F$	−2H		6
	n.d.	17.19	17.16	no HR-MS	400.16806 (3.37)	400.16873 (5.00)	12.0	$C_{21}H_{23}O_4N_3F$	−2H		6
	n.d.	n.d.	17.57	no HR-MS	no HR-MS	no HR-MS					
	20.09	20.52	20.40*	no HR-MS	400.16799 (3.20)	no HR-MS	12.0	$C_{21}H_{23}O_4N_3F$	−2H		6
401	16.34	16.49	16.53	402.18303 (1.66)	402.18413 (4.40)	402.18289 (1.31)	11.0	$C_{21}H_{25}O_4N_3F$			MOX
415	10.52*	10.74	10.58	no HR-MS	no HR-MS	no HR-MS					
	14.17	14.38	14.32	416.16137 (−0.62)	416.16150 (−0.3)	no HR-MS	12.0	$C_{21}H_{23}O_5N_3F$	−2H	+O	7
	16.94	17.40	17.28	no HR-MS	no HR-MS	no HR-MS					
	n.d.	21.46	21.40	no HR-MS	no HR-MS	no HR-MS					
	n.d.	n.d.	24.30	no HR-MS	no HR-MS	no HR-MS					
	n.d.	n.d.	24.98	no HR-MS	no HR-MS	no HR-MS					
417	13.70*	13.91*	13.76	no HR-MS	no HR-MS	418.17917 (4.53)	11.0	$C_{21}H_{25}O_5N_3F$		+O	1–5
	14.23*	14.47*	14.32	no HR-MS	no HR-MS	no HR-MS					
	n.d.	n.d.	15.23	no HR-MS	no HR-MS	418.17776 (1.16)	11.0	$C_{21}H_{25}O_5N_3F$		+O	1–5
	15.60	16.00	15.85	418.17582 (−3.48)	418.17722 (−0.14)	418.17997 (6.44)	11.0	$C_{21}H_{25}O_5N_3F$		+O	1–5
	n.d.	n.d.	17.60	no HR-MS	no HR-MS	no HR-MS					
429	11.89	12.11	n.d.	no HR-MS	430.14151 (1.44)	no HR-MS	13.0	$C_{21}H_{21}O_6N_3F$	−4H	+2O	9
	14.41	n.d.	14.92	no HR-MS	no HR-MS	no HR-MS					
	16.95	17.16	16.79	no HR-MS	430.14062 (0.63)	no HR-MS	13.0	$C_{21}H_{21}O_6N_3F$	−4H	+2O	9

[a] The numbering follows the proposed pathway (Fig. 3).
[b] HPLC retention time based on MS detection.
[c] Difference between measured and theoretical mass.
[d] DBE: Double Bond Equivalent.
* 3 < S/N < 10, n.d.: S/N < 3.

same nominal mass but different chromatographic retention times. High resolution measurements were performed for reaction solution samples taken at 95 min for pH 3.0, 65 min for pH 7.0 and 35 min for pH 10.0. The selected time at pH 10.0 allowed to perform a HR-MS analysis on additional peaks corresponding to a mass of 417 Da. Measured masses ($[M+H]^+$) and molecular compositions are presented in Table 2. Similar photoproducts are identified for all investigated pH levels. All detected compounds show a limited change in the UV-spectrum compared to MOX (Fig. SI-3). A large absorbance peak between 270 and 290 nm with a shoulder between 310 and 330 nm indicates that the quinolone core is unaffected and, by consequence, degradation occurs at the R_7 substituent [23]. This statement is supported by the fact that all detected degradation products retain at least two nitrogen atoms as well as the fluorine atom.

Structures are proposed based on the molecular formula, double bond equivalent (DBE) and molecular composition of the mother compound (Fig. 3). Compounds 1, 2, 7, 9, 11 and 12 are analogous to previously reported degradation products of fluoroquinolones using oxidation techniques, such as ozonation, photolysis, biodegradation and electrochemical oxidation [17,24–31]. Compounds 2, 7 and 9 have been earlier identified during MOX photocatalysis [10], but it is the first time that compounds 1, 3, 4, 5, 6, 8, 10, 11 and 12 are reported as MOX degradation products during heterogeneous photocatalysis.

Based on all identified reaction products, a pathway for the photocatalytic degradation of MOX is proposed in Fig. 3. Considering Table 2, up to five different degradation products with a mass of 417 Da are detected during MOX photocatalysis. Chromatographic retention times indicate that they consist of five different structures and HR-MS analysis shows a net gain of one oxygen atom compared to MOX. Compounds 1–5, as shown in Fig. 3, are all plausible structures for these detected degradation products. Among them, compounds 1 and 2 represent a ring cleavage of the cyclopropyl group or a random addition of a hydroxyl group, while compounds 3–5 have a ring cleavage on the (4a*S*,7a*S*)-octahydro-6*H*-pyrrolo[3,4-b]pyridin-6-yl, R_7, group. Hubicka et al. [29] observed a similar MOX degradation product with a ring opening on the R_7 group during photolytic treatment. Together with compound 6, formation of a double bound on the R_7 substituent, and compound 7, formation of a keto group on the R_7 substituent, these are probably the primary reaction products formed during photocatalytic degradation of MOX. Further oxidation can lead to the formation of a double keto group like compound 9 or the further degradation of the substituent resulting in compound 8. Degradation from compounds 8, 10 and 11 includes oxidation, reduction and demethylation reactions, eventually resulting in compound 12, which contains only the MOX quinolone moiety.

Using ab initio molecular orbital calculations, De Witte et al. [32] investigated where the most reactive centra for levofloxacin, a similar FQ, are positioned. From these calculations it could be concluded that the C_2 carbon and the N'_1 nitrogen are the most reactive centra in this molecule, with C_2 being a suitable site for hydroxyl radical attack, see Fig. 1. Since no degradation at the quinolone moiety has been observed in this study, one might conclude that the effect of hydroxyl radicals is negligible and that the main degradation mechanism occurs through reaction with holes or via direct charge injection as proposed by Paul et al. [33]. However, Van Doorslaer et al. [22] noticed that hydroxyl radicals contribute for about 24% in the degradation of MOX under UV-A irradiation using the same catalyst concentration. Degradation products formed by hydroxyl radical attack may be less stable, rapidly degrading into lower molecular weight compounds or are not easily detected by the applied HPLC-HR-MS methodology [17]. This might also explain why, so far, only one reference published two photocatalytic degradation products of a FQ, ciprofloxacin, resulting from a ring opening at the quinolone moiety [26].

Since no pH dependency is noticed in the main type of degradation products formed, the suggested pathway can be acknowledged as a general pathway for all pH levels. Nevertheless a pH effect is observed in the time profiles of the reaction products (Fig. 2, SI-1 and SI-2). The relative importance of the identified compounds in the liquid phase as a function of pH, in terms of maximum peak area observed during photocatalytic degradation, is presented in Fig. 4. Among the investigated pH levels, compounds 8, 9, 10 and 11 show the highest occurrence at neutral conditions. On the other hand, compounds 1–5, 6 and 7 show higher peak areas at pH 3.0 and 10.0 compared to pH 7.0. No significant pH influence on the formation of compound 12 could be observed. A clear shift in maximum abundance from 'weakly' oxidized degradation products at pH 3.0 and 10.0 toward more oxidized degradation products in neutral conditions is noticed.

A possible reason for this difference could be the influence of pH on the reaction speeds in the pathway favoring specific reactions or slowing down others, creating 'bottle-necks'. Another possible explanation can be found in the complex nature of the photocatalytic process itself. The photocatalytic degradation reaction of MOX takes place in the liquid phase and at the catalyst surface and is greatly influenced by pH. It has been shown in recent studies that the adsorption of FQs on a TiO_2 catalyst surface is higher at neutral conditions indicating that surface reactions are more pronounced [11,27,33]. The pH dependent adsorption of MOX together with the formation of degradation products, which probably have a similar pH dependent adsorption behavior, could contribute to the different distribution of degradation products.

In order to fully elucidate the mechanisms taking place and the applicability of the degradation technique, experiments should also be performed at environmental relevant concentrations and in real effluent matrices.

3.2. Residual antibacterial activity

As demonstrated in Section 3.1, MOX is subject to photocatalytic degradation, and mineralization is incomplete. The efficiency of the photocatalytic treatment is not solely defined by the chemical degradation of MOX, but also by the reduction of the residual antibacterial activity of the reaction solution. Therefore, agar diffusion tests are performed with a selection of bacteria from the antibacterial spectrum of MOX. In a first step, the sensitivity of the bacteria strains is evaluated using a concentration range of MOX (0–12.46 μM). The dose–response curve of MOX for the selected bacteria is presented in Fig. 5 (full symbols). In a second step, agar diffusion tests are performed on photocatalytic samples using the methodology mentioned in Section 2.4. The inhibition zone diameters resulting from the samples of the photocatalytically treated solution at pH 7.0 are also plotted in Fig. 5 (open symbols). For *K. pneumoniae*, *S. carnosus* and *S. mutans* similar inhibition zone diameters are attained for a given standard MOX concentration and a similar MOX concentration during photocatalytic degradation. This correlation indicates that the mother compound is the main descriptor for the residual antibacterial activity. A similar trend is noticed for the FQs levofloxacin and ciprofloxacin, the residual antibacterial activity of the photocatalytically treated solutions correlated well with the residual amount of mother compound in solution [17,19]. For *E. coli* the observed inhibition zone diameters, resulting from the photocatalytic samples, are slightly higher than the inhibition zone diameters for a given MOX concentration between 0 and 8 μM MOX (Fig. 5). This may indicate that *E. coli* is more sensitive to the formed degradation products of MOX.

In a third step, the residual percentage of inhibition, based on the measured inhibition zone diameters, for the selected bacteria

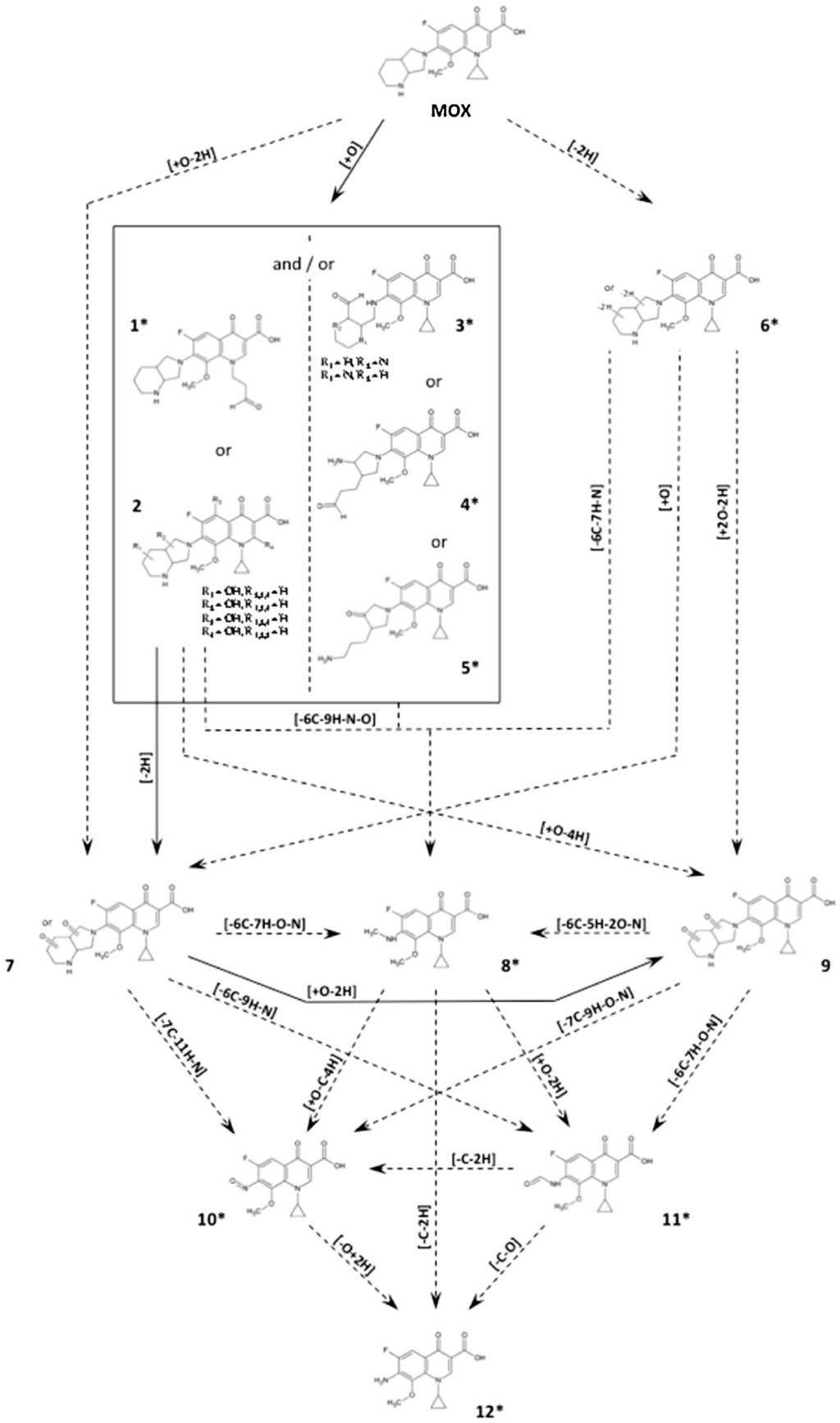

Fig. 3. Proposal of the initial photocatalytic degradation pathway of MOX. Compounds marked with * are newly identified MOX photocatalytic degradation products. Dashed lines are newly proposed possible degradation routes, in addition to the full lines described in literature [10]. Multiple plausible structures are proposed for compounds 6, 7 and 9 due to the unknown exact location of the double bond and keto functions, respectively.

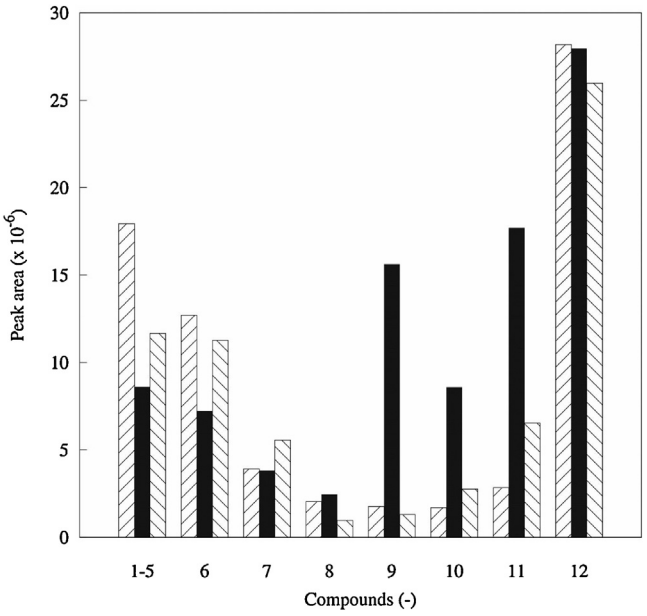

Fig. 4. Maximum LR-MS peak areas detected in the liquid phase of compounds 1–12 during photocatalytic degradation of MOX as a function of pH 3.0: ▨; 7.0: ■; and 10.0: ▧. With $C_{0,MOX}$ = 124.6 μM, C_{cat} = 1.0 g L^{-1}, T = 298 K, 13.2 rps and 60 ml min^{-1} air (n_{rep} = 1).

during photocatalytic degradation of MOX at pH 3.0, 7.0 and 10.0 is compared (Table 3). Photographs of the inhibition zones for *S. carnosus* for the investigated pH levels are illustrated in supporting information (Fig. SI-4). After 12 min of photocatalytic treatment of MOX at pH 7.0 no residual antibacterial activity is noticed for all investigated bacteria. Residual activity is still observed after 14 min of reaction under acidic and alkaline conditions, probably due to the slower photocatalytic degradation rate of MOX at these pH levels as discussed in Section 3.1 [11].

All degradation products observed during photocatalytic degradation of MOX retain the quinolone structure, see Section 3.1. This quinolone core contains a carboxyl and a keto group which are considered to be essential for the antibacterial activity since they are necessary for the FQ-DNA gyrase binding [34]. Hence, the degradation of this moiety could be supposed to be necessary to reduce the antibacterial activity. Therefore, we could expect higher inhibition zone diameters resulting from the photocatalytic degradation samples comparing to the inhibition zone diameters resulting from the MOX concentration range, but this was not the case as demonstrated in Fig. 5. Transformation and/or degradation of the auxiliary groups, such as the R_7 group, can also significantly decrease the antibacterial activity [35]. Chu and Fernandes [34] reported that quinolones with a large substituent at the R_7 position have a higher activity than the ones with a smaller group at that position. This is also shown by Wetzstein et al. [36] who have found that desethylene ciprofloxacine is 100 fold less active than its mother compound against *E. coli* and that the base quinolone core of ciprofloxacin has less than 3% of the antibacterial activity compared to ciprofloxacin. A similar compound retaining only the MOX quinolone moiety is identified during photocatalytic treatment of

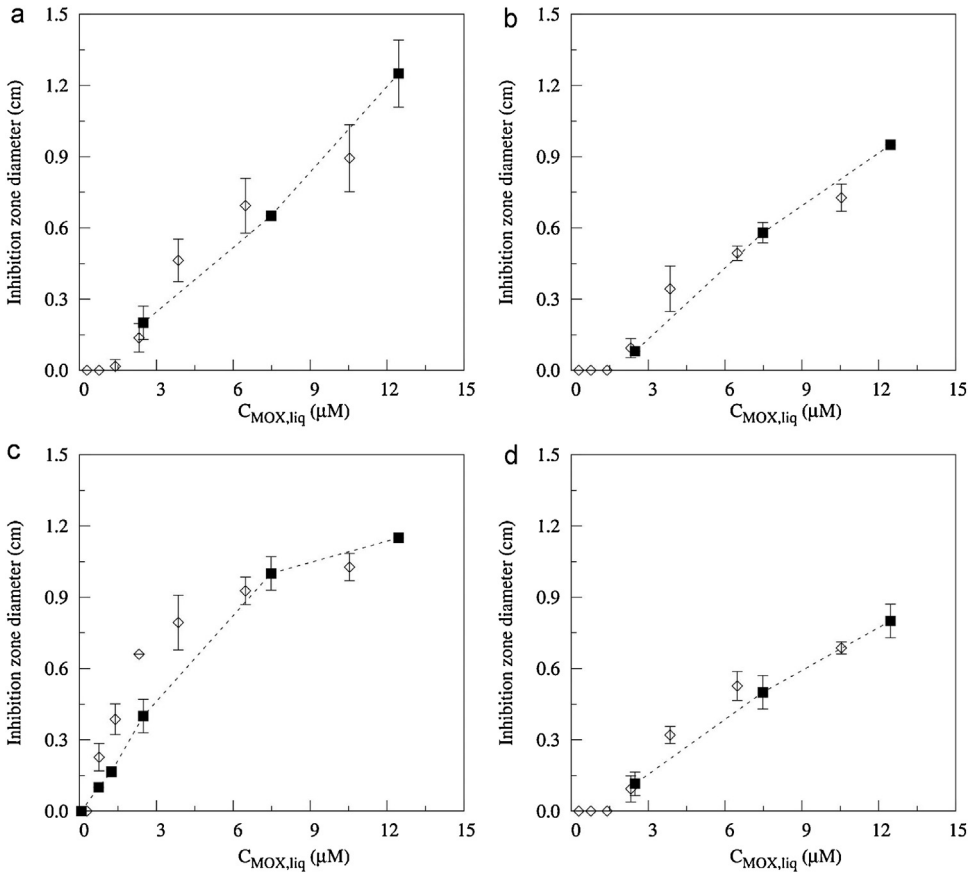

Fig. 5. Inhibition zone diameters (n_{rep} = 3) as a function of MOX concentrations 0.07, 0.75, 1.25, 2.49, 7.48 and 12.46 μM (■) for *K. pneumoniae* (a), *S. mutans* (b), *E. coli* (c) and *S. carnosus* (d) together with the inhibition zone diameters as a function of the MOX concentration of the 1/3 diluted photocatalytic degradation samples (◊) after 12, 10, 8, 6, 4, 2, and 0′ min of degradation time ($C_{0,MOX}$ = 37.4 μM, C_{cat} = 1.0 g L^{-1}, pH 7.0, T = 298 K, 13.2 rps and 60 ml min^{-1} air; n_{rep} = 3). Dashed line is plotted to guide the eye.

Table 3
Percentage of residual antibacterial activity based on inhibition zone diameters versus photocatalytic degradation time at pH 3.0, 7.0 and 10.0 (C_{cat} = 1.0 g L^{-1}, $C_{0,MOX}$ = 37.4 μM, T = 298 K; 60 mL min^{-1} air, 13.2 rps) for *K. pneumoniae* (G^-), *S. mutans* (G^+), *E. coli* (G^-) and *S. carnosus* (G^+). Time 0′ representing the starting point for the reaction after adsorption/desorption equilibrium. Photocatalytic reaction samples were 1/3 diluted before addition of 20 μL. Inhibition diameters were measured after an aerobic incubation of 48 h at 37 °C. Standard deviations are based on triplicate measurements (n_{rep} = 3).

Species	pH	Reaction time (min)							
		0‘	2	4	6	8	10	12	14
K. pneumoniae	3	100.0	96.1 ± 1.6	90.3 ± 2.9	77.5 ± 9.7	70.1 ± 14.9	64.8 ± 14.5	54.1 ± 17.1	49.4 ± 21.3
	7	100.0	77.3 ± 3.2	51.6 ± 3.7	16.1 ± 9.3	–[a]	–	–	–
	10	100.0	88.6 ± 0.4	78.0 ± 2.2	72.5 ± 6.4	61.5 ± 6.9	54.0 ± 6.7	48.2 ± 11.0	32.9 ± 9.6
S. mutans	3	100.0	95.8 ± 4.1	89.0 ± 6.1	82.6 ± 1.1	75.0 ± 7.8	72.8 ± 11.3	63.3 ± 7.5	53.7 ± 7.4
	7	100.0	68.0 ± 2.0	46.8 ± 10.1	13.1 ± 6.6	–	–	–	–
	10	100.0	93.4 ± 0.4	76.5 ± 4.3	64.5 ± 4.3	53.3 ± 5.2	40.4 ± 4.2	27.8 ± 5.9	15.4 ± 6.5
E. coli	3	100.0	93.3 ± 5.8	91.6 ± 5.9	84.7 ± 7.6	88.3 ± 3.1	86.2 ± 4.0	79.3 ± 7.5	77.9 ± 5.5
	7	100.0	90.2 ± 0.6	77.0 ± 7.1	64.4 ± 3.7	37.6 ± 5.1	21.9 ± 4.5	–	–
	10	100.0	98.4 ± 2.7	93.0 ± 6.2	89.5 ± 1.1	82.5 ± 6.5	77.1 ± 5.4	71.7 ± 8.4	60.4 ± 2.0
S. carnosus	3	100.0	87.4 ± 3.2	81.9 ± 1.4	74.0 ± 2.4	70.7 ± 3.9	72.8 ± 6.4	61.5 ± 12.0	41.3 ± 18.5
	7	100.0	76.6 ± 7.2	46.7 ± 6.3	13.4 ± 7.7	–	–	–	–
	10	100.0	90.8 ± 3.5	81.1 ± 3.3	66.2 ± 3.0	44.3 ± 12.2	37.7 ± 8.5	28.9 ± 8.6	14.0 ± 10.6

[a] Below visual detection.

MOX (Compound 12, Fig. 3). Next to the altered activity, a reduced binding affinity with DNA topoisomerases is achieved because the R_7 substituent is an important factor for target selection by quinolones [37].

Overall, the evaluation of the antibacterial activity of a single degradation product is difficult to determine. It is more relevant to evaluate the potential of a photocatalytic treatment technique through the assessment of the overall bacterial inhibition after a given reaction time. Since a different trend in decrease of antibacterial activity has been noticed for the investigated bacteria, the importance to evaluate the efficiency of a degradation process in real applications for a large variety of bacterial species has to be emphasized. According to Lemaire et al. [38], a different sensitivity is not only noticed between different species, but also between different strains of one bacterial species. Therefore, conclusions for one bacterial species have to be made with caution, keeping in mind the interspecies variation of sensitivity.

4. Conclusions

The photocatalytic degradation of MOX has been evaluated. In a first part the detection and identification of degradation products is performed at different pH conditions. At neutral pH a more efficient MOX removal is achieved than working under acidic or alkaline conditions. Time profiles of the different degradation products are plotted and reveal that the solution pH influences the abundance of the different degradation products in the water phase during reaction. Nonetheless the same main photocatalytic degradation products are observed at all pH levels. All the detected degradation products in this study retain the base quinolone moiety. A new pathway is proposed with the different degradation products resulting in a better understanding of the photocatalytic degradation mechanism of MOX.

In a second part, the residual antibacterial activity of the reaction solution is determined. By linking inhibition zone diameters resulting from a MOX concentration range with the inhibition zone diameters of photocatalytic samples, it is clear that the residual concentration of mother compound in solution correlates well with the residual antibacterial activity for all investigated bacterial species. *E. coli* is slightly more sensitive toward the formed degradation products since in a higher inhibition zone diameter is observed for the photocatalytic samples. Heterogeneous photocatalysis is very effective in reducing the antibacterial activity at pH 7.0. No residual antibacterial activity could be observed for the four investigated bacterial species after 12 min of degradation time. Photocatalysis is therefore a promising technique to degrade the antibiotic MOX and to reduce its antibacterial activity in wastewater effluents decreasing the resistance formation potential.

Appendix A. Supplementary data

Supplementary data associated with this article can be found, in the online version, at http://dx.doi.org/10.1016/j.apcatb.2013.03.011.

References

[1] A. Speltini, M. Sturini, F. Maraschi, A. Profumo, Journal of Separation Science 33 (2010) 1115–1131.
[2] K. Kummerer, Journal of Environment Management 90 (2009) 2354–2366.
[3] D. Fatta-Kassinos, S. Meric, A. Nikolaou, Analytical and Bioanalytical Chemistry 399 (2011) 251–275.
[4] K.L. Jury, S.J. Khan, T. Vancov, R.M. Stuetz, N.J. Ashbolt, Critical Reviews in Environment Science and Technology 41 (2011) 243–270.
[5] K. Kummerer, A. Henninger, Clinical Microbiology and Infection 9 (2003) 1203–1214.
[6] G. Carlsson, S. Orn, D.G.J. Larsson, Environmental Toxicology and Chemistry 28 (2009) 2656–2662.
[7] I. Ebert, J. Bachmann, U. Kuehnen, A. Kuester, C. Kussatz, D. Maletzki, C. Schlueter, Environmental Toxicology and Chemistry 30 (2011) 2786–2792.
[8] E. De Bel, J. Dewulf, B. De Witte, H. Van Langenhove, C. Janssen, Chemosphere 77 (2009) 291–295.
[9] B. De Witte, H. Van Langenhove, K. Demeestere, K. Saerens, P. De Wispelaere, J. Dewulf, Chemosphere 78 (2010) 1142–1147.
[10] M. Sturini, A. Speltini, F. Maraschi, A. Profumo, L. Pretali, E.A. Irastorza, E. Fasani, A. Albini, Applied Catalysis B: Environmental 119 (120) (2012) 32–39.
[11] X. Van Doorslaer, K. Demeestere, P.M. Heynderickx, H. Van Langenhove, J. Dewulf, Applied Catalysis B: Environmental (2011) 540–547.
[12] P.M. Heynderickx, K. Demeestere, J. Dewulf, B. De Witte, H. Van Langenhove, Journal of Advanced Oxidation Technologies 14 (2011) 71–80.
[13] T.G. Vasconcelos, K. Kummerer, D.M. Henriques, A.F. Martins, Journal of Hazardous Materials 169 (2009) 1154–1158.
[14] N. Adriaenssens, S. Coenen, A. Versporten, A. Muller, G. Minalu, C. Faes, V. Vankerckhoven, M. Aerts, N. Hens, G. Molenberghs, H. Goossens, Journal of Antimicrobial Chemotherapy 66 (2011) 47–56.
[15] C. Sirtori, A. Zapata, W. Gernjak, S. Malato, A. Agüera, Chemosphere 88 (2012) 627–634.
[16] E. Hapeshi, A. Achilleos, M.I. Vasquez, C. Michael, N.P. Xekoukoulotakis, D. Mantzavinos, D. Kassinos, Water Research 44 (2010) 1737–1746.
[17] T. Paul, M.C. Dodd, T.J. Strathmann, Water Research 44 (2010) 3121–3132.
[18] D. Fatta-Kassinos, M.I. Vasquez, K. Kuemmerer, Chemosphere 85 (2011) 693–709.
[19] D. Nasuhoglu, A. Rodayan, D. Berk, V. Yargeau, Chemical Engineering Journal 189–190 (2012) 41–48.
[20] B. De Witte, H. van Langenhove, K. Demeestere, J. Dewulf, Critical Reviews in Environment Science and Technology 41 (2011) 215–242.
[21] R.A. Spurr, H. Myers, Analytical Chemistry 29 (1957) 760–762.
[22] X. Van Doorslaer, P.M. Heynderickx, K. Demeestere, K. Debevere, H. Van Langenhove, J. Dewulf, Applied Catalysis B: Environmental 111 (2012) 150–156.
[23] M.H. Langlois, M. Montagut, J.P. Dubost, J. Grellet, M.C. Saux, Journal of Pharmaceutical and Biomedical Analysis 37 (2005) 389–393.
[24] B. De Witte, J. Dewulf, K. Demeestere, V.V. De Vyvere, P. De Wispelaere, H. Van Langenhove, Environmental Science and Technology 42 (2008) 4889–4895.

[25] E. Guinea, J.A. Garrido, R.M. Rodriguez, P.L. Cabot, C. Arias, F. Centellas, E. Brillas, Electrochimica Acta 55 (2010) 2101–2115.
[26] P. Calza, C. Medana, F. Carbone, V. Giancotti, C. Baiocchi, Rapid Communications in Mass Spectrometry 22 (2008) 1533–1552.
[27] T.C. An, H. Yang, G.Y. Li, W.H. Song, W.J. Cooper, X.P. Nie, Applied Catalysis B: Environmental 94 (2010) 288–294.
[28] J. Burhenne, M. Ludwig, P. Nikoloudis, M. Spiteller, Environmental Science and Pollution Research 4 (1997) 10–15.
[29] U. Hubicka, J. Krzek, B. Zuromska, M. Walczak, M. Zylewski, D. Pawlowski, Photochemical & Photobiological Sciences 11 (2012) 351–357.
[30] W. Karl, J. Schneider, H.G. Wetzstein, Applied Microbiology and Biotechnology 71 (2006) 101–113.
[31] H.G. Wetzstein, N. Schmeer, W. Karl, Applied and Environment Microbiology 63 (1997) 4272–4281.
[32] B. De Witte, H. Van Langenhove, K. Hemelsoet, K. Demeestere, P. De Wispelaere, V. Van Speybroeck, J. Dewulf, Chemosphere 76 (2009) 683–689.
[33] T. Paul, P.L. Miller, T.J. Strathmann, Environmental Science and Technology 41 (2007) 4720–4727.
[34] D.T.W. Chu, P.B. Fernandes, Antimicrobial Agents and Chemotherapy 33 (1989) 131–135.
[35] P.C. Sharma, A. Jain, S. Jain, Acta Poloniae Pharmaceutica 66 (2009) 587–604.
[36] H.G. Wetzstein, M. Stadler, H.V. Tichy, A. Dalhoff, W. Karl, Applied and Environment Microbiology 65 (1999) 1556–1563.
[37] F.L. Alovero, X.S. Pan, J.E. Morris, R.H. Manzo, L.M. Fisher, Antimicrobial Agents and Chemotherapy 44 (2000) 320–325.
[38] S. Lemaire, P.M. Tulkens, F. Van Bambeke, Antimicrobial Agents and Chemotherapy 55 (2011) 649–658.